AIIM

Association for Information and Image Management

1100 Wayne Avenue, Suite 1100
Silver Spring, Maryland 20910

301/587-8202

Centimeter

1 2 3 4 5 6 7 8 9 10 11 12 13 14 15 mm

1 2 3 4 5

Inches

1.0 1.1 1.25 1.4 1.6 1.8 2.0 2.2 2.5 2.8 3.2 3.6 4.0 4.5 5.0 5.6 6.3 7.1 8.0

1 of 1

Conf-930702--38

Implementation of an Anisotropic Turbulence Model in the COMMIX-1C/ATM Computer Code*

by

M. Bottoni and F. C. Chang
Materials and Components Technology Division
Argonne National Laboratory
9700 South Cass Avenue
Argonne, Illinois 60439

Submitted to the 1993 ASME Pressure Vessels and Piping (PVP) Division Conference, Denver, CO, July 25-29, 1993

*Work sponsored by Laboratory Directed Research and Development Funds, Argonne National Laboratory

IMPLEMENTATION OF AN ANISOTROPIC TURBULENCE MODEL IN THE COMMIX-1C/ATM COMPUTER CODE

M. Bottoni and F. C. Chang
Materials and Components Technology Division
Argonne National Laboratory
9700 South Cass Avenue
Argonne, IL 60439, USA
(708) 252-6094

ABSTRACT

The computer code COMMIX-1C/ATM, which describes single-phase, three-dimensional transient thermofluiddynamic problems, has provided the framework for the extension of the standard k-ε turbulence model to a six-equation model with additional transport equations for the turbulence heat fluxes and the variance of temperature fluctuations. The new model, which allows simulation of anisotropic turbulence in stratified shear flows, is referred to as the Anisotropic Turbulence Model (ATM). The ATM has been verified with numerical computations of stable and unstable stratified shear flow between parallel plates.

INTRODUCTION

Computational analysis of the inherent safety capabilities of advanced reactors requires modeling of three-dimensional anisotropic turbulence in stratified flows. The objective is to prove through computational analysis that even in the worst case of loss of power to the primary pumps, natural convection circulation provides a power sink (through intermediate heat exchangers) sufficient to prevent coolant temperatures from reaching saturation.

For this purpose, the two-equation k-ε turbulence model has been implemented in the COMMIX-1C[1] computer program with three additional equations for turbulence heat fluxes and one additional equation for variance of temperature fluctuations. The resulting model allows simulation of the anisotropy of turbulence. The performances of the new model have been evaluated by simulating Viollet's thermal stratification experiments[2] and by comparing the numerical results with those obtained by applying the standard k-ε model. The results show that in the case of unstable thermal stratification, in which buoyancy forces become important, the anisotropic turbulence model performs better than the k-ε model.

This article presents the details of the anisotropic turbulence model, its analytical and numerical treatments, and the verification performed so far.

k–ε TWO-EQUATION TURBULENCE MODEL

The transport equations describing the time and space distribution of the turbulence kinetic energy k and its dissipation ε are

$$\rho\frac{\partial k}{\partial t} + \rho U_j\frac{\partial k}{\partial x_j} = P_k + G_k - \rho\varepsilon + \frac{\partial}{\partial x_j}\left[\left(\frac{\mu_t}{\sigma_k} + \mu_\ell\right)\frac{\partial k}{\partial x_j}\right], \tag{1}$$

$$\rho\frac{\partial \varepsilon}{\partial t} + \rho U_j\frac{\partial \varepsilon}{\partial x_j} = c_{1\varepsilon}\frac{\varepsilon}{k}(P_k + G_k)(1 + c_{3\varepsilon}R_f) - c_{2\varepsilon}\rho\frac{\varepsilon^2}{k} + \frac{\partial}{\partial x_j}\left[\left(\frac{\mu_t}{\sigma_\varepsilon} + \mu_\ell\right)\frac{\partial \varepsilon}{\partial x_j}\right]. \tag{2}$$

Figures 1 and 2 show the two–layer wall function model used in COMMIX–1C/ATM. When $y_p > y_\ell$, the first node is in the fully turbulent zone and one has

$$k_p = u^{*2}/\sqrt{c_\mu}, \tag{3}$$

$$\varepsilon_p = u^{*3}/(Ky_p), \tag{4}$$

$$u^* = KU_p/\ell n(Ey_p u^*/\nu_\ell). \tag{5}$$

When $y_p \le y_\ell$, the node P is in the laminar sublayer and one has

$$k_p = u^{*2}(y_p/y_\ell)/\sqrt{c_\mu}, \tag{6}$$

$$\varepsilon_p = u^{*3}/(Ky_\ell). \tag{7}$$

ANISOTROPIC TURBULENCE MODEL (ATM)

This model uses, beyond the k–ε equations given above, three additional transport equations for turbulence heat fluxes and one additional equation for variance of temperature fluctuations. The transport equations for the scalar fluxes are[3]

$$\frac{\partial(\overline{u_i\phi})}{\partial t} + U_j\frac{\partial(\overline{u_i\phi})}{\partial x_j} = \frac{\partial}{\partial x_j}\left[\left(\nu_\ell + \frac{\nu_t}{\sigma_\phi}\right)\frac{\partial(\overline{u_i\phi})}{\partial x_j}\right] - \left(\overline{u_iu_j}\frac{\partial T}{\partial x_j} + \overline{u_j\phi}\frac{\partial U_i}{\partial x_j}\right) - \beta g_i\overline{\phi^2} + \pi_{i\phi}. \tag{8}$$

The four terms on the right side of eq. (8) are diffusive transport, mean–field production, buoyancy production, and pressure gradient correlation, respectively. The Reynold stresses $\overline{u_iu_j}$ in eq. (8) are computed by

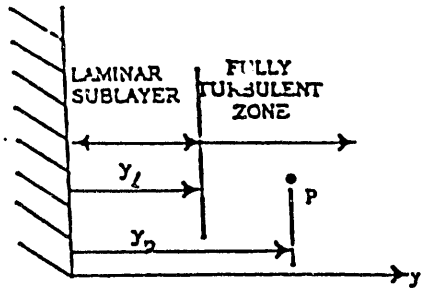

Fig. 1. Two-layer wall-function model ($y_p > y\ell$)

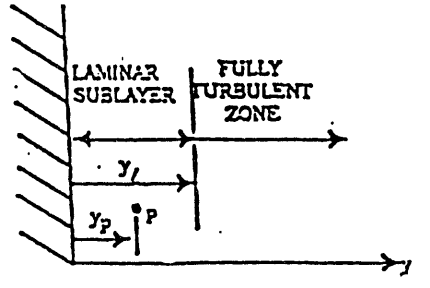

Fig. 2. Two-layer wall-function model ($y_p \leq y\ell$)

$$\overline{u_i u_j} = \left(\overline{u_i u_j}\right)_{k-\varepsilon} + \left(\overline{u_i u_j}\right)_{ASM} = -\nu_t\left(\frac{\partial U_i}{\partial x_j} + \frac{\partial U_j}{\partial x_i}\right) + \frac{2}{3}\delta_{ij}\,k + C_s\frac{k}{\rho\varepsilon}\,\frac{G_{ij} - \frac{2}{3}\delta_{ij}G_k}{c_1 + (P_k + G_k)/\rho\varepsilon - 1} \tag{9}$$

with

$$G_{ij} = -\rho\beta\left(g_i\overline{u_j\phi} + g_j\overline{u_i\phi}\right). \tag{10}$$

The first two terms on the right-hand side of eq. (9) are used for the computation of the Reynolds stresses in the standard k-ε model. The last term adds a contribution which takes into account the anisotropy of the distribution of the turbulence kinetic energy. This last term is a slight modification of the form suggested in Ref. 4. The constant C_s (= 2~3) has been chosen so that the order of magnitude of the $(\overline{u_i u_j})_{ASM}$ term in the direction of the gravity g_i, ($g_j = 0$ for $j \neq i$) is the same as that of the term $(\overline{u_i u_j})_{k-\varepsilon}$. It is important to remark that the choice of the modeling for the $(\overline{u_i u_j})_{ASM}$ terms does not affect the turbulence kinetic energy, because $(\overline{u_i u_i})_{ASM} = 0$ (summation implied).

The pressure gradient $\pi_{i\phi}$ is computed by

$$\pi_{i\phi} = \frac{1}{\rho}\overline{p\frac{\partial\phi}{\partial x_i}} = -c_{1\phi}\frac{\varepsilon}{k}\overline{u_i\phi} + c_{2\phi}\overline{u_j\phi}\frac{\partial U_i}{\partial x_j} + c_{3\phi}\beta g_i\overline{\phi}^2 - c'_{1\phi}\overline{u_n\phi}\delta_{in}f\left(\frac{L}{x_n}\right). \quad (11)$$

The four terms in eq. (11) are the main turbulence, mean strain, buoyancy, and wall contributions, respectively. The last term was formulated according to Ref. 5.

Transport Equation for Variance of Temperature Fluctuations

The transport equation for the variance of temperature fluctuations $\overline{\phi}^2$ is

$$\frac{\partial\overline{\phi}^2}{\partial t} + U_j\frac{\partial\overline{\phi}^2}{\partial x_j} = \frac{\partial}{\partial x_j}\left(c'_\phi\frac{k^2}{\varepsilon}\frac{\partial\overline{\phi}^2}{\partial x_j}\right) + \frac{\partial}{\partial x_j}\left(\frac{\lambda}{\rho c_p}\frac{\partial\overline{\phi^2}}{\partial x_j}\right) - 2\overline{u_j\phi}\frac{\partial T}{\partial x_j} - \frac{\varepsilon}{k}\frac{\overline{\phi^2}}{R}. \quad (12)$$

The terms on the right side of eq. (12) are turbulence diffusion, molecular diffusion, mean production, and dissipation, respectively.

Boundary Conditions

The boundary conditions adopted for the scalar fluxes are

$$\left(\overline{u_i\phi}\right)_p = C_\mu\frac{k^2}{\varepsilon}\frac{\partial T}{\partial x_i}, \ (i = 1,2,3) \quad (13)$$

$$-\overline{u_i\phi} = -\frac{\lambda}{\rho c_p}\frac{\partial T}{\partial x_i} = -\frac{\mu_t}{\rho\sigma_t}\frac{\partial T}{\partial x_i}, \quad (14)$$

for $y_p \le y_\ell$ and $y_p > y_\ell$, respectively.

The boundary conditions for the variance of temperature fluctuations are

$$g_p\left(v_p\frac{y_\ell}{y_p} + \frac{\Gamma_{g\ell}}{y_\ell - y_p} + \frac{\Gamma_{gp}}{y_p}\right) = \Gamma_{g\ell}\frac{g_\ell}{y_\ell - y_p} + \Gamma_{gp}\frac{g_w}{y_p} + \frac{(u^*T^*)^2\sigma_t}{2\nu_t}y_\ell - \frac{c_g^2}{R\nu_\ell}(u^*T^*)^2 y_\ell, \quad (15)$$

$$g_w = R\sigma_t T^{*2}/\sqrt{c_\mu}, \quad (16)$$

for $y_p \le y_\ell$ and $y_p > y_\ell$, respectively. Equation (16) has been derived by integrating a one-dimensional transport equation, written for a coordinate normal to the wall, over the laminar boundary layer thickness.

More details about the derivation of the transport equations used and about the treatment of the boundary conditions are given in Ref. 6.

The numerical values used for the constants have been determined by experiments[3,7] and are as follows: $c_1 = 1.8$, $c_\mu = 0.09$, $c_{1\varepsilon} = 1.44$, $c_{2\varepsilon} = 1.92$, $c_{3\varepsilon} = 0.8$, $c'_\phi = 0.13$, $c_{1\phi} = 3.1$, $c'_{1\phi} = 0.5$, $c_{2\phi} = 0.5$, $c_{3\phi} = 0.5$, $E = 9.0$, $K = 0.42$, $R = 0.5$, $\sigma_k = 1.0$, $\sigma_t = 0.9$, $\sigma_\varepsilon = 1.3$, $\sigma_\phi = 1.3$, and $c_g = 1$.

NUMERICAL TREATMENT OF TRANSPORT EQUATIONS

All of the above equations can be written in the following generalized form:

$$\frac{\partial \Phi}{\partial t} + \frac{\partial}{\partial x_j} J_{\phi j} = S_\Phi \tag{17}$$

with the following definitions:

i) For the k–equation

$$\Phi = \rho k, \tag{18a}$$

$$J_{\phi j} = \rho k U_j - \left(\frac{\mu_t}{\sigma_k} + \mu_\ell\right)\frac{\partial k}{\partial x_j}, \tag{18b}$$

$$S\Phi = P_k + G_k - \rho\varepsilon; \tag{18c}$$

ii) For the ε–equation

$$\phi = \rho\varepsilon, \tag{19a}$$

$$J_{\phi j} = \rho\varepsilon U_j - \left(\frac{\mu_t}{\sigma_\varepsilon} + \mu_\ell\right)\frac{\partial \varepsilon}{\partial x_j}, \tag{19b}$$

$$S\Phi = c_{1\varepsilon}\frac{\varepsilon}{k}(P_k + G_k)(1 + c_{3\varepsilon}R_f) - c_{2\varepsilon}\rho\frac{\varepsilon^2}{k}; \tag{19c}$$

iii) For the $u_i\phi$–equations

$$\Phi_i = \overline{u_i\phi}, \tag{20a}$$

$$J_{\phi j i} = U_j(\overline{u_i\phi}) - \left(\nu_\ell + \frac{\nu_t}{\sigma_\phi}\right)\frac{\partial(\overline{u_i\phi})}{\partial x_i}, \tag{20b}$$

$$S_{\Phi_i} = -\left(\overline{u_i u_j}\frac{\partial T}{\partial x_j} + \overline{u_j\phi}\frac{\partial U_i}{\partial x_j}\right) - \beta g_i\overline{\phi^2} + \pi_{i\phi}; \tag{20c}$$

iv) For the $\overline{\phi^2}$–equation

$$\Phi = \overline{\phi^2}. \tag{21a}$$

$$J_{\phi j} = U_j\overline{\phi^2} - \left(c_\phi' \frac{k^2}{\varepsilon}\frac{\partial\overline{\phi^2}}{\partial x_j} + \frac{\lambda}{\rho c_p}\frac{\partial\overline{\phi^2}}{\partial x_j}\right). \tag{21b}$$

$$S_\Phi = -2\overline{u_j\phi}\frac{\partial T}{\partial x_j} - \frac{\varepsilon}{k}\frac{\overline{\phi^2}}{R}. \tag{21c}$$

Integration of eq. (17) over a control volume centered on nodes i, j, k and application of the divergence theorem yield

$$\int_{V_f}[\partial(\rho\Phi)/\partial t]dV + \int_{A_{f,i+1/2}} J_{\phi i}dA - \int_{A_{f,i-1/2}} J_{\phi i}dA + \int_{A_{f,j+1/2}} J_{\phi j}dA$$
$$- \int_{A_{f,j-1/2}} J_{\phi j}dA + \int_{A_{f,k+1/2}} J_{\phi k}dA - \int_{A_{f,k-1/2}} J_{\phi k}dA = \int_{V_f} S_\Phi dV. \tag{22}$$

Using the definitions of the mean values of the flux J_ϕ over the bounding surfaces and of mean values over the fluid volume V_f, we transform eq. (22) into an algebraic equation for the seven unknowns Φ_β (β = 0, 1, ..., 6) at time level t_{n+1}:

$$a_o\Phi_o^{n+1} + \sum_{\beta=1}^{6} a_\beta\Phi_\beta^{n+1} = b_o^n. \tag{23}$$

The subscript o in eq. (23) refers to the center node (i, j, k) considered, while β refers to the neighboring nodes in the three coordinate directions. The right-hand side of eq. (23) collects all terms at time level t_n.

Equation (23) is solved for all transport equations with direct numerical methods.

RESULTS AND DISCUSSION

The ability to model buoyancy effects and stratified flow phenomena is of high importance in many reactor problems. A very simple experiment designed to study the effect of buoyancy on turbulent mixing is the case of a horizontal shear flow, as shown in Fig. 3. The influence of buoyancy is measured by the reduced Froude number

$$F_r = \frac{|\overline{U}_2 - \overline{U}_1|}{\sqrt{g_i\beta h|T_2 - T_1|}}. \tag{24}$$

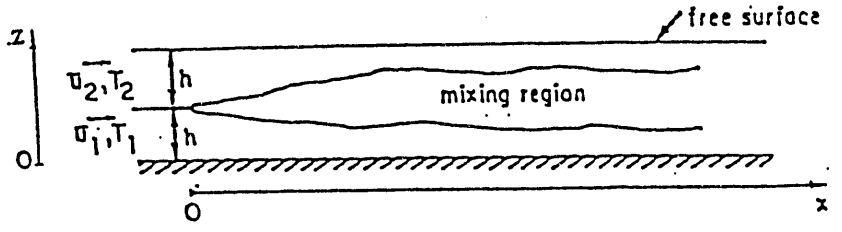

Fig. 3. Sketch of stratified shear flow

In stable stratification, when the hot fluid enters at the top, gravity forces oppose the diffusive character of turbulence, which tends to mix the fluids despite the density differences. The smaller the Froude number, the more stable the stratification. Beyond some threshold of the Froude number, turbulence is completely inhibited by the density gradients. In unstable stratification, when the hot fluid enters at the bottom, the effects of gravity and of turbulence combine, thus forcing a region of highly effective mixing between the hot and cold fluids.

In this study, we used 100 meshes in the axial direction along the channel length and 30 meshes in the transverse direction. The length–to–height ratio (x_{max}/h) is 30. Density effects are obtained by hot and cold water with different inlet velocities. Momentum continuity is assumed at the exit plane. We discuss results of two test cases with stable or unstable stratification and Froude number 0.9.

In the stable stratified shear flow (hot fluid injected in the upper half, $\overline{U}_1 = 2\overline{U}_2$ and $T_2 > T_1$), turbulent mixing is inhibited by buoyancy effects. Computed results obtained by using the k–ε two–equation turbulence model and the anisotropic turbulence model are shown in Figs. 4–6.

Figure 4 shows the profiles of axial velocity at location x/h = 20. The results from the anisotropic turbulence model are close to those from the k–ε turbulence model. Figure 5 shows the temperature distributions at location x/h = 20. Despite weak mixing, the temperature of the upper layer of the cold fluid has slightly increased from the inlet value. The difference between the k–ε model and the anisotropic model is more significant at the exit.

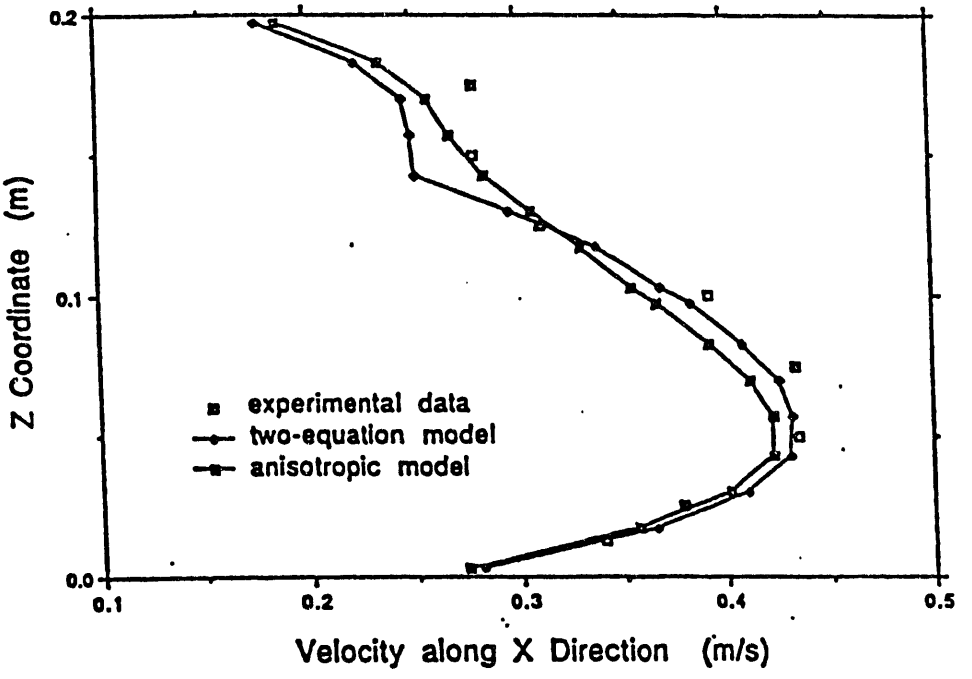

Fig. 4. Velocity profiles for stable stratified shear flow at x/h = 20

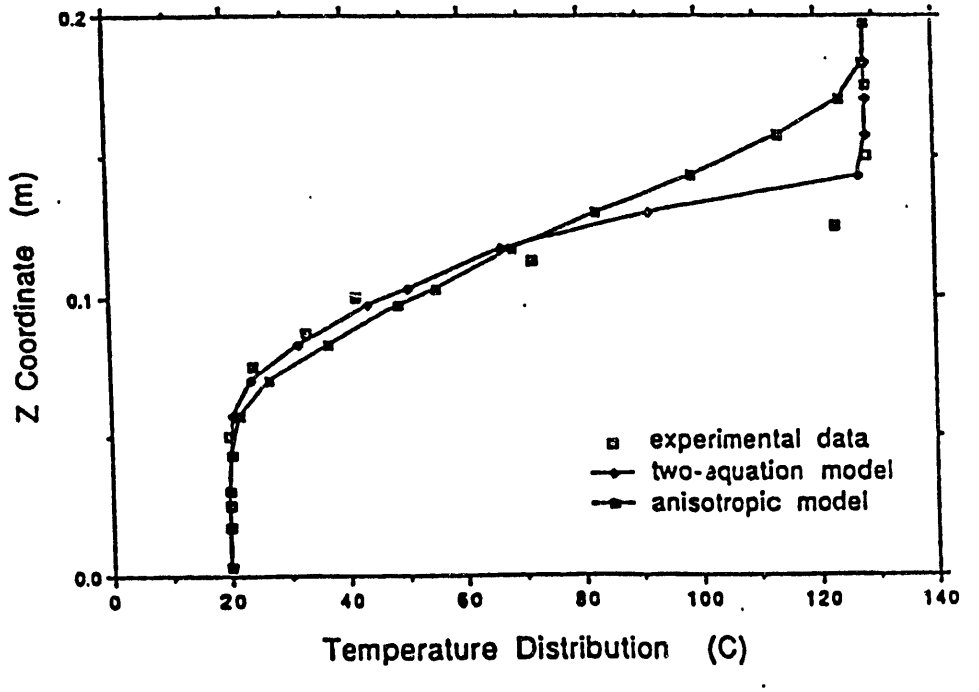

Fig. 5. Temperature distributions for stable stratified shear flow at x/h = 20

Figure 6 represents the variance of temperature fluctuations ($g = 0.5\ \overline{\phi^2}$) at axial location x/h = 10 and x/h = 20 for the anisotropic turbulence model. In the case of stable mixing, the temperature fluctuation ($\bar{\phi}$) is about 13.4°C and seems to be within a reasonable range when compared with the inlet temperature difference [$13.4/(T_2 - T_1) = 12.3\%$]. In the anisotropic turbulence model used, the computed values of the $\overline{u_i\phi}$ turbulence heat fluxes are of paramount importance because of their impact on the buoyancy contribution G_k to the turbulence kinetic energy.

In the unstable stratified shear flow (hot water injected at the lower half, $\overline{U}_1 = 2\overline{U}_2$ and $T_2 < T_1$), very strong mixing is observed. Computed results, obtained by using the k–ε two–equation turbulence model and the anisotropic turbulence model, are shown in Figs. 7–12.

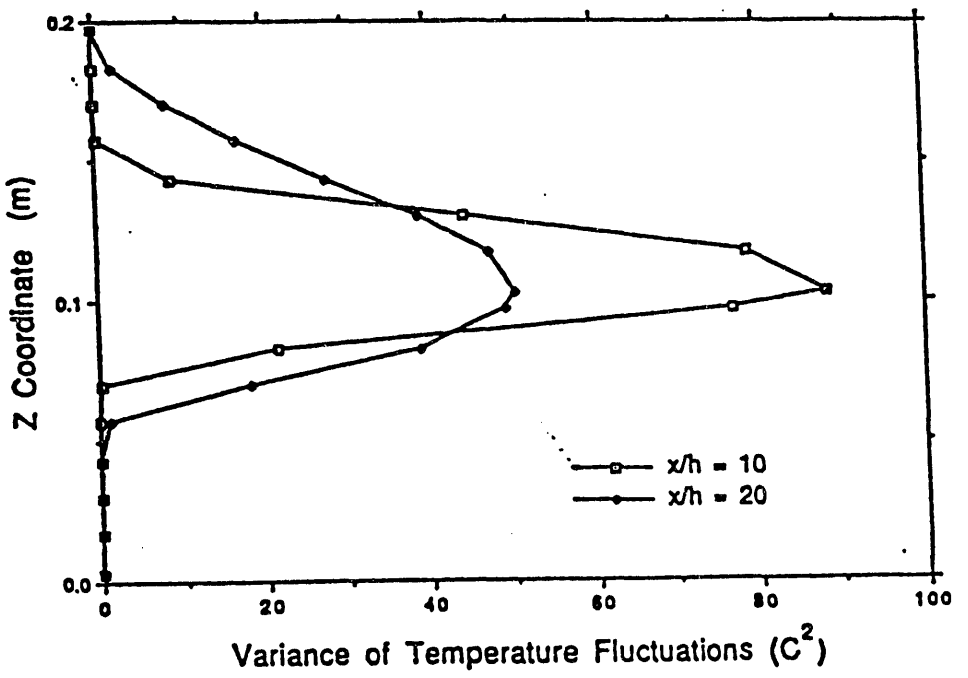

Fig. 6. Variance of temperature fluctuations for stable stratified shear flow at x/h = 10 and x/h = 20

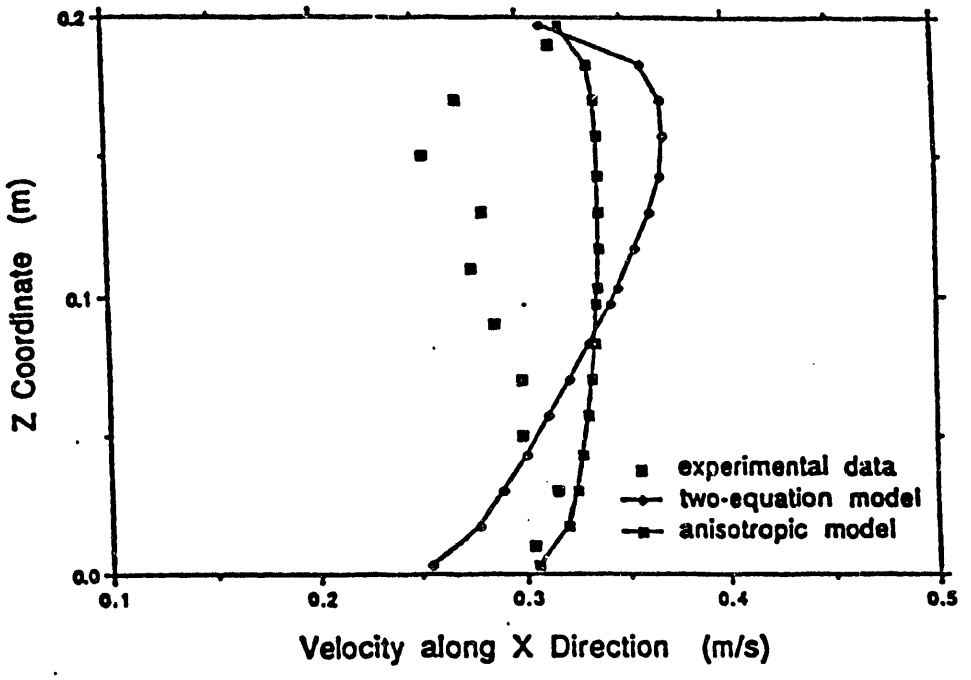

Fig. 7. Velocity profiles for unstable stratified shear flow at x/h = 20

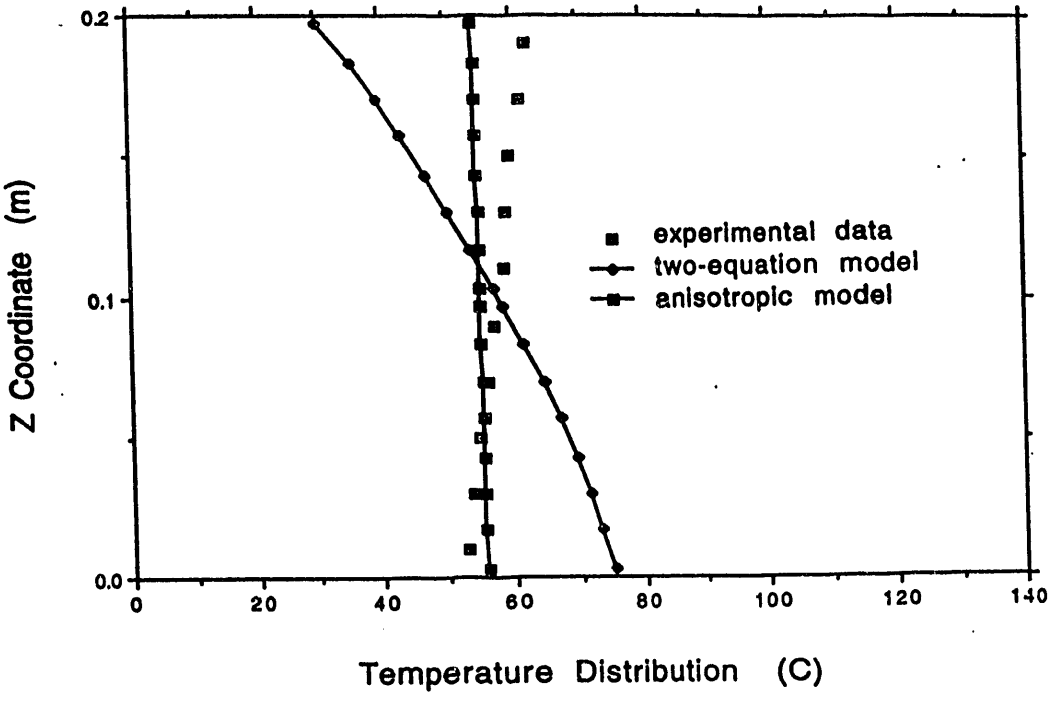

Fig. 8. Temperature distributions for unstable stratified shear flow at x/h = 20

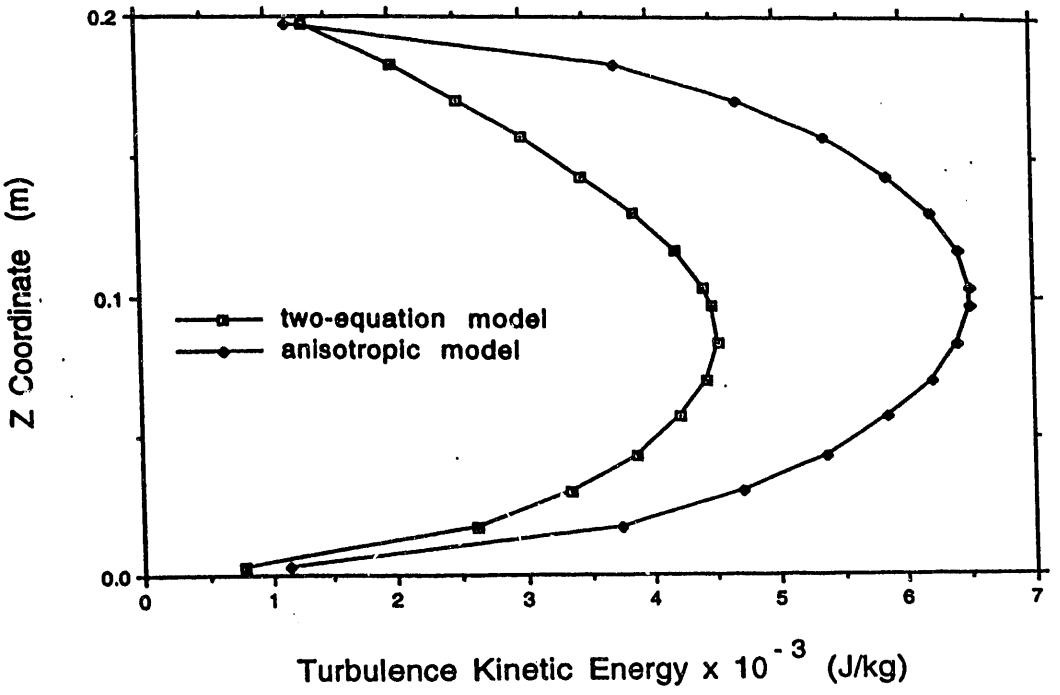

Fig. 9. Turbulence kinetic energy for unstable stratified shear flow at x/h = 20

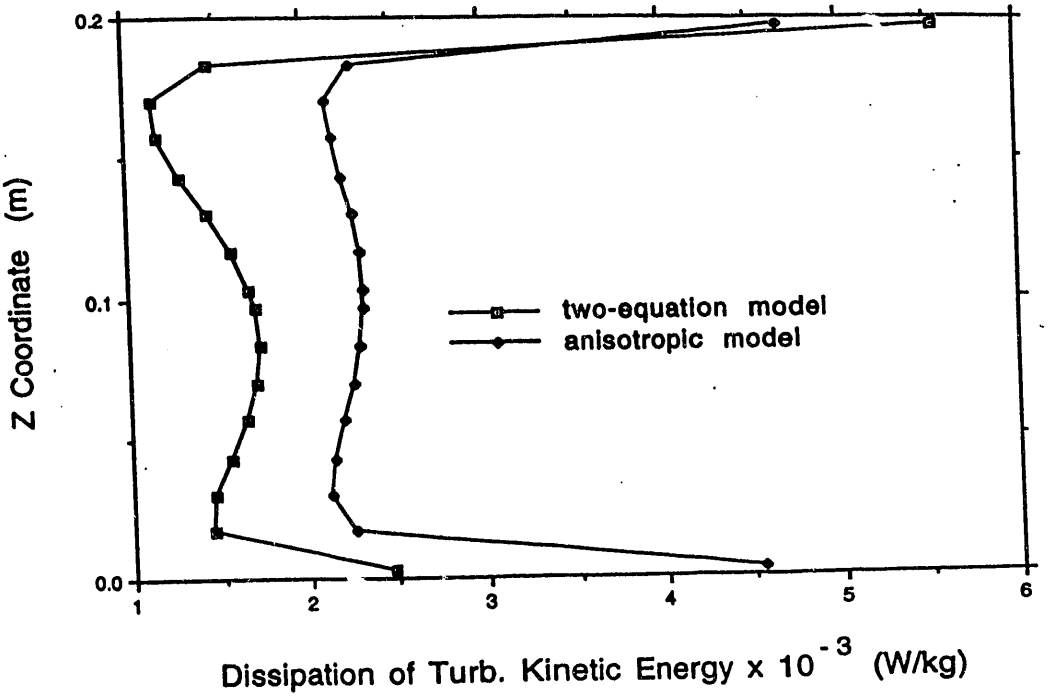

Fig. 10. Dissipation of turbulence kinetic energy for unstable stratified shear flow at x/h = 20

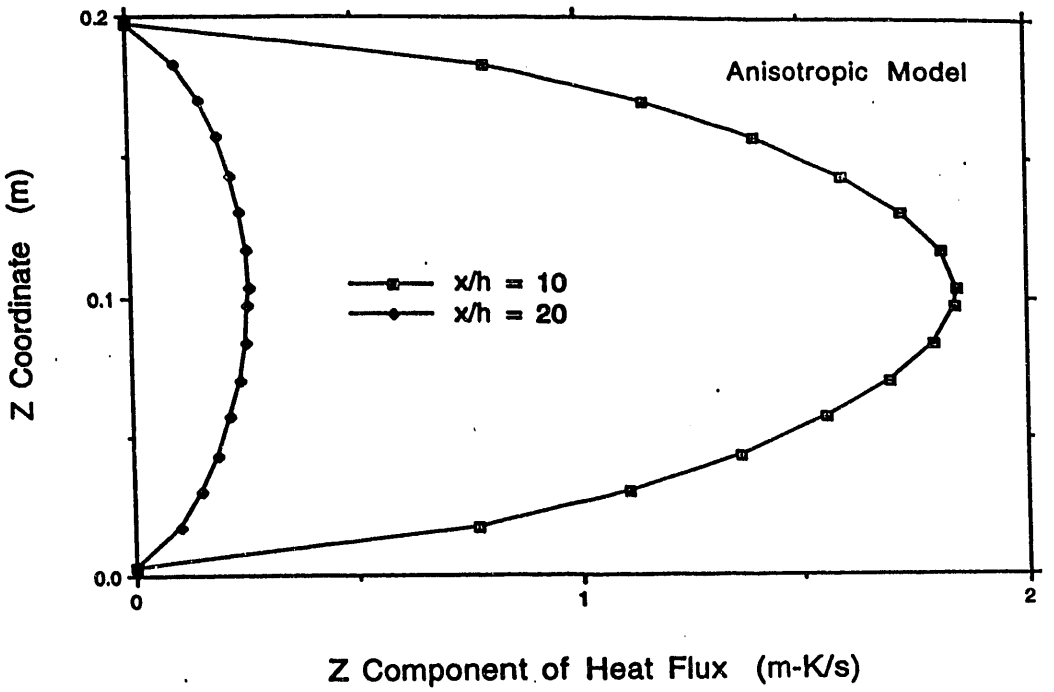

Fig. 11. Turbulence heat flux ($\overline{w\phi}$) for unstable stratified shear flow at x/h = 10 and x/h = 20

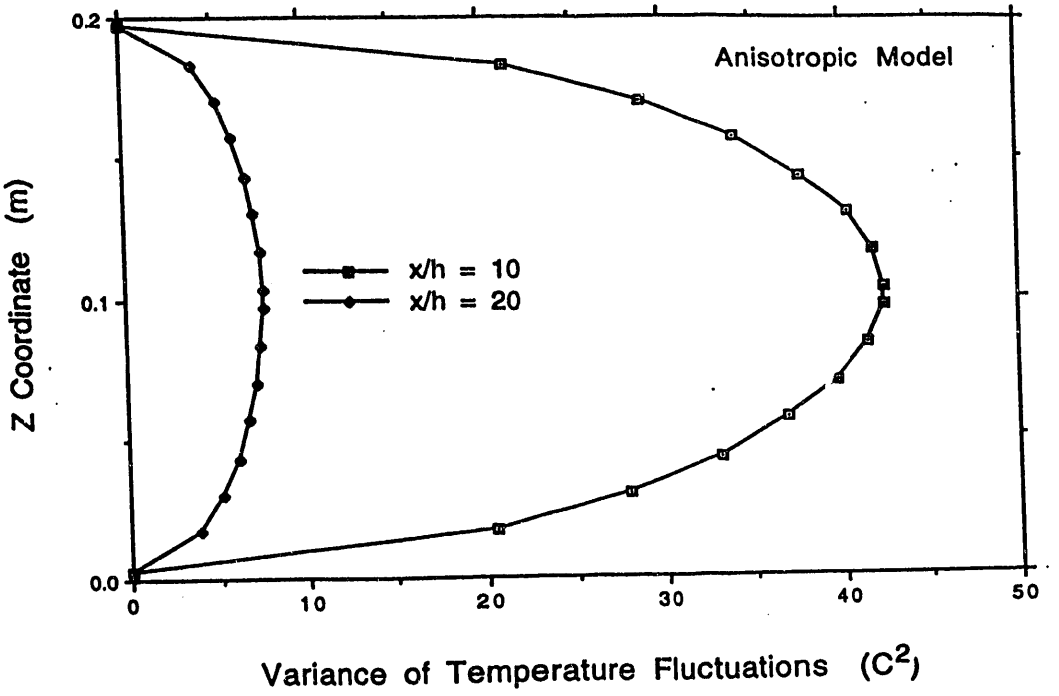

Fig. 12. Variance of temperature fluctuations for unstable stratified shear flow at x/h = 10 and x/h = 20

Figure 7 shows the profiles of axial velocity at location x/h = 20. Because the mixing effect is enhanced by buoyancy along the channel, the velocity difference between cold water and hot water is decreased. The results from the anisotropic turbulence model are closer to the experimental results than those from the k–ε turbulence model. The still remaining discrepancy between the experimental data and the results obtained with the anisotropic turbulence model are probably due to the approximation made in the computation of the Reynolds stresses, and thus hint to the future work necessary to further improve the modeling.

Figure 8 shows the temperature distributions at location x/h = 20. With strong mixing, the temperature distributions in hot and cold fluids also reach almost the same values. Compared with the k–ε turbulence model, the anisotropic turbulence model can produce results closer to the experimental results by taking into account the anisotropy behaviors of natural circulation and turbulence transport. The mixing effect in unstable stratified flow is stronger than that in stable stratified flow because the buoyancy force in the unstable case is dominant.

The distributions of k at location x/h = 20 are shown in Fig. 9. The distributions of ε at the same location are displayed in Fig. 10. These two figures show that along the channel, both k and ε are transported from the interface to the interior of the fluids by natural circulation and turbulence. The values of k and ε from the anisotropic turbulence model are higher than those from the k–ε turbulence model. This is because in the anisotropic model, stronger contributions to the production of turbulence kinetic energy come from buoyancy.

Figure 11 shows the distribution of turbulence heat flux in the transverse direction normal to the channel walls at axial locations x/h = 10 and x/h = 20 for the anisotropic turbulence model. At location x/h = 10, the heat flux has its maximum value at the interface of the two fluids, and then at location x/h = 20 the distribution becomes flatter because strong mixing has already occurred upstream from this location.

Figure 12 represents the variance of temperature fluctuations ($g = 0.5\ \overline{\phi^2}$) at axial locations x/h = 10 and x/h = 20 for the anisotropic turbulence model. The variance has a higher value at the interface of two fluids at x/h = 10 and becomes uniform downstream of

the channel at x/h = 20 due to the formation of developed flow. The maximum temperature fluctuation ($\bar{\phi}$) at x/h = 10 is about 9°C and seems to be within a reasonable range when compared with the inlet temperature difference [$\bar{\phi}/(T_2 - T_1) = 7\%$].

SUMMARY AND FUTURE DEVELOPMENT

The standard k–ε two–equation turbulence model, which assumes isotropic turbulence, performs poorly in buoyancy–induced natural circulation phenomena. To account for the nonisotropic effects of the turbulence due to buoyancy, we improved the two–equation model by adding four additional transport equations for the turbulence heat fluxes and for the variance of temperature fluctuations. The resulting anisotropic turbulence model has been tested in stable and unstable stratified flows. In the case of stable stratification, the anisotropic model essentially reproduces the results of the k–ε model. In the case of unstable stratification, where the k–ε model performs poorly, the anisotropic model gives results in better agreement with experimental data. The remaining discrepancy is probably due to the simplifications made in evaluating the Reynolds stresses. Future work, therefore, aims at modeling more accurately the Reynolds stresses or at computing them rigorously with additional transport equations.

ACKNOWLEDGMENTS

This work has been sponsored by Laboratory Directed Research and Development Funds granted by the Argonne National Laboratory. The COMMIX–1C code, developed in the past years by colleagues Drs. H. M. Domanus, T. H. Chien, and J. G. Sun, and by Section Manager Dr. W. T. Sha, has provided the framework for the incorporation of the new anisotropic turbulence model. Best thanks are due to Mrs. S. Moll for her accurate work in typing the manuscript.

NOMENCLATURE

A_f Surface area (m^2)

c_p Specific heat (J/kg–K)

E Constant characterizing the roughness of a boundary surface

F_r Froude number

G_{ij} Components of buoyancy tensor ($kg/m\text{-}s^3$)

G_k Production or suppression of turbulence kinetic energy due to buoyancy ($J/s\text{-}m^3$)

g $\left(=\frac{1}{2}\overline{\phi^2}\right)$, one half of variance of temperature fluctuations (g_w = value at the wall)(K^2)

g_i Components of gravitational acceleration (m/s^2)

J_ϕ Convective and diffusive vector (dimensions depending on equation considered)

k Turbulence kinetic energy (J/kg)

K von Karman constant

L Length scale (m)

P_k Mean shear production in k and ε equations ($J/s\text{-}m^3$)

p Pressure (N/m^2)

q_w Heat flux from surface [$J/(s\text{-}m^2)$]

R_f $(= - G_k/P_k)$, Richardson number

S_Φ Generalized source term (dimensions depending on equation considered)

t time (s)

T Temperature (K)

T^* $q_w/\rho c_p u^*$ (K)

U_i Components of mean velocity (m/s)

u_i Velocity fluctuations (m/s)

u_n Fluctuation of velocity component normal to the wall (m/s)

u^* Friction velocity (m/s)

$\overline{u_i\phi}$ Heat flux (m K/s)

$\overline{u_iu_j}$ Reynolds stresses (m^2/s^2)

V_f Fluid volume in a cell (m^3)

x_i Coordinate directions (m)

x_n Distance from the wall (m)

y_ℓ Thickness of laminar sublayer (m)

y_p Distance of node P from the wall (m)

Greek

β $\left[= -\frac{1}{\rho}\left(\frac{\partial \rho}{\partial T}\right)_p\right]$, volume expansion coefficient at constant pressure (K^{-1})

$\Gamma_{g\ell}$ Laminar diffusivity at location y_ℓ (m^2/s)

Γ_{gp} Laminar diffusivity at location y_p (m^2/s)

δ_{ij} Kronecker delta

ε Dissipation of turbulence kinetic energy (W/kg)

λ Thermal conductivity (W/mK)

μ_ℓ Laminar dynamic viscosity (kg/m–s)

μ_t Turbulence dynamic viscosity (kg/m–s)

ν_ℓ Laminar kinematic viscosity (m^2/s)

ν_t Turbulence kinematic viscosity (m^2/s)

$\pi_{i\phi}$ Pressure–scalar gradient correlation in scalar flux equations (m K/s^2)

ρ Density (kg/m^3)

σ_k Turbulence Prandtl number for k

σ_t Turbulence Prandtl number for heat transport

σ_ε Turbulence Prandtl number for ε

$\bar{\phi}$ Temperature fluctuations (K)

Φ Transported physical quantity (dimensions depending on equation considered)

Indices

ASM Anisotropic turbulence model

i,j,k (=1, 2, 3) Coordinate direction

f Fluid

ℓ Laminar

n Normal to wall

p Value at node P

t Turbulent

w Wall

REFERENCES

1. H.M. Domanus et al., *COMMIX–1C: A Three–Dimensional Transient Single–Phase Computer Program for Thermal Hydraulic Analysis of Single–Component and Multicomponent Engineering Systems. Volume I: Equations and Numerics; Volume II: User's Guide and Manual*, NUREG/CR–5649, ANL–90/33 (November 1990).

2. P.L. Viollet, *Turbulent Mixing in a Two Layer Stratified Shear Flow*, Second Int. Symp. on Stratified Flows, Trondheim, Norway, pp. 315–325 (June 24–27, 1980).

3. W. Rodi, *Turbulence Models and Their Application in Hydraulics – A State of the Art Review*, Int. Assoc. for Hydraulics Research (IAHR), Delft, The Netherlands (June 1980).

4. L. Davidson, *Second–Order Corrections of the k–ε Model to Account for Non–isotropic Effects due to Buoyancy*, Int. J. Heat Mass Transfer 33:12, pp. 2599–2608 (1990).

5. M.M. Gibson and B.E. Launder, *Ground Effects on Pressure Fluctuations in the Atmospheric Boundary Layer*, J. Fluid Mech. 86, part 3, pp. 491–511 (1978).

6. F. C. Chang, M. Botttoni, and W. T. Sha, *Development and Validation of the k–ε Two–Equation Turbulence Model and the Six–Equation Anisotropic Turbulence Model in the COMMIX Code (COMMIX–1C/ATM)*, ANL/ATHRP–44 (Jan. 1992).

7. C. J. Chen and S. Y. Jaw, *Present Status and Future Approach of Turbulence Modeling*, Research Paper, Department of Mechanical Engineering, University of Iowa (Oct, 1983).

DATE
FILMED
8/17/93
END